Clinical Cancer Research

Functional Parameters Derived from Magnetic Resonance Imaging Reflect Vascular Morphology in Preclinical Tumors and in Human Liver Metastases

Pavitra Kannan[1], Warren W. Kretzschmar[2], Helen Winter[1], Daniel Warren[1], Russell Bates[3], Philip D. Allen[1], Nigar Syed[1,4], Benjamin Irving[3], Bartlomiej W. Papiez[3], Jakob Kaeppler[1], Bosjtan Markelc[1], Paul Kinchesh[1], Stuart Gilchrist[1], Sean Smart[1], Julia A. Schnabel[3,5], Tim Maughan[1], Adrian L. Harris[1], Ruth J. Muschel[1], Mike Partridge[1], Ricky A. Sharma[1,6], and Veerle Kersemans[1]

Abstract

Purpose: Tumor vessels influence the growth and response of tumors to therapy. Imaging vascular changes *in vivo* using dynamic contrast-enhanced MRI (DCE-MRI) has shown potential to guide clinical decision making for treatment. However, quantitative MR imaging biomarkers of vascular function have not been widely adopted, partly because their relationship to structural changes in vessels remains unclear. We aimed to elucidate the relationships between vessel function and morphology *in vivo*.

Experimental Design: Untreated preclinical tumors with different levels of vascularization were imaged sequentially using DCE-MRI and CT. Relationships between functional parameters from MR (*i*AUC, K^{trans}, and BAT_{frac}) and structural parameters from CT (vessel volume, radius, and tortuosity) were assessed using linear models. Tumors treated with anti-VEGFR2 antibody were then imaged to determine whether antiangiogenic therapy altered these relationships. Finally, functional–structural relationships were measured in 10 patients with liver metastases from colorectal cancer.

Results: Functional parameters *i*AUC and K^{trans} primarily reflected vessel volume in untreated preclinical tumors. The relationships varied spatially and with tumor vascularity, and were altered by antiangiogenic treatment. In human liver metastases, all three structural parameters were linearly correlated with *i*AUC and K^{trans}. For *i*AUC, structural parameters also modified each other's effect.

Conclusions: Our findings suggest that MR imaging biomarkers of vascular function are linked to structural changes in tumor vessels and that antiangiogenic therapy can affect this link. Our work also demonstrates the feasibility of three-dimensional functional–structural validation of MR biomarkers *in vivo* to improve their biological interpretation and clinical utility. *Clin Cancer Res; 24(19); 4694–704. ©2018 AACR.*

Introduction

Solid tumors develop complex vascular networks during their growth. This vascular network not only provides nutrients and oxygen supply to tumor cells, but also plays a critical role in response to treatment. Changes in the vascular structure and function can alter blood flow, which can affect the delivery of chemotherapeutics to the tumor, as well as result in regions of hypoxia that can change the response of the tumor to radiotherapy (1, 2). Noninvasive imaging of these changes during the course of treatment could aid cancer physicians to guide clinical decisions and refine treatment (3, 4).

Dynamic contrast-enhanced MRI (DCE-MRI) is a noninvasive, functional technique that can image vascular changes *in vivo*. These changes are quantified from the uptake and distribution of a bolus of contrast agent injected intravenously, resulting in parameters such as the volume transfer constant (K^{trans}), the initial area under the curve of contrast uptake up to a predetermined time point (*i*AUC), and the fraction of voxels enhancing at the time of bolus arrival (BAT_{frac}; refs. 3, 5). Changes in these imaging biomarkers have been used to monitor pharmacodynamic changes in response to antiangiogenic treatment and to measure biological changes that occur in tumor vessels (6–10).

[1]CRUK and MRC Oxford Institute for Radiation Oncology Department of Oncology, University of Oxford, Oxford, United Kingdom. [2]School of Engineering Sciences in Chemistry, Biotechnology and Health, Department of Gene Technology, Science for Life Laboratory, KTH Royal Institute of Technology, Stockholm, Sweden. [3]Institute of Biomedical Engineering, Department of Engineering Science, University of Oxford, Oxford, United Kingdom. [4]NHS, Department of Radiology, Churchill Hospital, Oxford, United Kingdom. [5]School of Biomedical Engineering and Imaging Sciences, King's College London, London, United Kingdom. [6]NIHR University College London Hospitals Biomedical Research Centre, University College London, London, United Kingdom.

Note: Supplementary data for this article are available at Clinical Cancer Research Online (http://clincancerres.aacrjournals.org/).

P. Kannan, W.W. Kretzschmar, and H. Winter are joint first authors of this article.

R.A. Sharma and V. Kersemans are joint last authors of this article.

Corresponding Author: Pavitra Kannan, University of Oxford, CRUK and MRC Oxford Institute for Radiation Oncology, Old Road Campus Research Building, Oxford OX3 7DQ, United Kingdom. Phone: 44-1865-857-124; E-mail: pk@sciencesylt.com

doi: 10.1158/1078-0432.CCR-18-0033

Translational Relevance

Parameters of tumor perfusion, such as *i*AUC and K^{trans}, from dynamic contrast-enhanced MRI have shown potential as biomarkers in clinical trials to predict tumor response to antiangiogenics and other adjuvant therapies. Unfortunately, the biological interpretation of these functional parameters with respect to changes in tumor vessel morphology remains unclear, in part because many studies compared functional changes that occur on a millimeter resolution in MR with structural changes that occur on a micrometer level in histology. By using *in vivo* imaging and three-dimensional analysis in preclinical and human tumors, we demonstrate a clinically feasible method that links functional MR parameters to structural features of vessels. We find that functional parameters reflect vessel morphology, that this dependence varies with vascularity and with region, and that the dependence is affected by antiangiogenic therapy. By linking functional parameters to structural ones, our findings could improve the biological interpretation of these biomarkers.

They have also been correlated with clinical outcome in many studies (11–17). However, these biomarkers have limited influence in clinical decision making because their relationship to changes at the morphologic level remains unclear (4, 18, 19), limiting the potential to adapt therapy in light of response. The linking of these MR parameters to morphologic changes in vessels (i.e., biological validation) would not only improve their utility in the clinic, but could also provide mechanistic insights into the biological actions exerted by cancer therapies (18–20).

Biological validation of these MR parameters to vessel morphology has conventionally been performed by correlating relationships between functional parameters (e.g., K^{trans}) derived from DCE-MRI scans with structural parameters (i.e., microvascular density) derived from histology. Although correlations have been found in some cancers (4), the results have been conflicting, in part because they compare MRI parameters derived from three-dimensional (3D) volumetric images with histologic parameters derived from derived from two-dimensional (2D) slices (4, 21). A recent consensus document identified incomplete imaging-biology validation as a major shortcoming in translating imaging biomarkers and strongly recommended the use of 3D techniques to improve comparisons between vessel function and structure (21).

In this study, we attempt to tackle this shortcoming by measuring the 3D relationship between functional imaging parameters and structural vascular features *in vivo* to facilitate clinical utility. To achieve this aim, we used improved imaging (22) and 3D segmentation techniques (23) to extract functional parameters derived from DCE-MRI and structural parameters derived from contrast-enhanced CT performed *in vivo*. Relationships were first assessed in untreated tumors from two different preclinical models with high and low levels of vascularization. We then tested whether these relationships reproduced in an independent cohort of mice and whether they were altered when tumors were treated with an antiangiogenic agent. Finally, we applied the methodology on imaging data from patients with liver metastases from colorectal cancer to test its clinical feasibility and to test whether the preclinical relationships held true for clinical data.

Materials and Methods

Cell lines

Two cell lines, mouse colon carcinoma MC38 and human pharyngeal carcinoma FaDu, were used for imaging experiments. MC38 cells, generated through chemical induction of colon carcinoma in C57BL/6 mouse strain, were a gift (Dr. Carlos Arteaga, Vanderbilt University). FaDu cells (original source ATCC) were analyzed by short tandem repeat profile analysis; cells matched the ATCC reference at 8/9 markers and Cancer Genome Project STR data at 13/13 markers (CRUK Cancer Centre Genomics Facility, Leeds, UK). Cells were checked regularly using MycoAlert Mycoplasma Detection Kit (Lonza) to ensure they were negative for mycoplasma. Details regarding cell culture conditions are in Supplementary Methods.

Animal models

To assess changes in vessel morphology and perfusion during tumor growth (cohort 1), we imaged C57BL/6 mice bearing MC38 tumors ($n = 16$) and nu/nu mice bearing FaDu tumors ($n = 13$). Each tumor model contained a range of tumor volumes (MC38: 74.7–646.9 mm^3 measured using CT; FaDu: 51.2–302.1 mm^3 measured using CT) to determine whether changes in vessel morphology and perfusion correlated with tumor growth. FaDu tumors larger than 400 mm^3 were not used because they had poor uptake of contrast agents, which made quantification of imaging parameters less reliable. Details regarding animals and tumor inoculation are provided in Supplementary Methods.

To determine whether vessel morphology and perfusion were altered with antiangiogenic treatment (cohort 2), C57BL/6 mice bearing MC38 tumors ($n = 12$ mice per group) were treated with anti-mouse VEGFR2 antibody (clone DC101, 500 μg/dose, 27 mg/kg, BioXCell) or Rat IgG1 (clone HRPN, 500 μg/dose, BioXCell). For *in vivo* microscopy experiments, C57BL/6 mice bearing MC38 tumors ($n = 4$ mice per group) were treated in the same way (24). Once tumors reached 30 mm^3, intraperitoneal injections were administered every 3 days for a total of two times (25). Tumors were imaged 6 days after start of treatment. No toxicity or adverse events were observed during the treatment. Procedures were conducted in accordance with the UK Animal Scientific Procedures Act of 1986 (Project License Number 30/2922) and were approved by the Committee on the Ethics of Animal Experiments at the University of Oxford.

Preclinical imaging

In vivo imaging using CT and DCE-MRI was performed using the immobilization and imaging setup previously described to detect vessel structure and perfusion in the same tumor regions (22). *In vivo* imaging of vessel perfusion using multiphoton microscopy was performed to corroborate results of *in vivo* CT after antiangiogenic treatment. Further details regarding instrument and scan settings are provided in Supplementary Methods.

Patients

Baseline imaging data from 10 patients (mean age ± SD, 66 ± 9 y; 8 males and two females) with liver metastases (mean volume ± SD, 250 ± 270 cm^3) from chemorefractory colorectal cancer were used for the clinical cohort. Patients were enrolled in the PERFORM clinical trial (NCT01410760) and selected based on published criteria (26). Written consent was obtained from all patients. Studies were conducted in accordance with Institutional

Research Review Board at the University of Oxford and the Berkshire Regional Ethics Committee (ref 09/H0505/1). The clinical trial sponsor was the University of Oxford.

Clinical imaging

Patients were injected intravenously with contrast agent (Omnipaque 300, 100 mL, 4 mL/s) and were scanned using an abdominal CT scan 30 seconds later (LightSpeed VCT, GE Medical Systems). CT images were acquired using X-ray tube settings of 120 kV, 307 μA, a 500-ms exposure per projection, and a voxel size of $0.85 \times 0.85 \times 0.63$ mm^3. MRI was performed on a 1.5T or 3T scanner (Signa HDxt; GE Medical Systems) with respiratory triggering. Anatomical and T1-weighted images were acquired for tumor segmentation and pharmacokinetic modeling. DCE-MR images were subsequently acquired using a 3D gradient echo sequence (TE = 2.12 ms, TR = 4.46 ms, flip angle = 12°, and voxel size = $0.9 \times 0.9 \times 2.5$ mm^3) after injection of contrast agent (ProHance® [Gadoteridol], 40 mL, 2 mL/s). Manual tumor segmentation was performed independently on CT and MRI scans.

Quantification of *in vivo* imaging parameters

Vessel segmentation was performed on CT images (22) to quantify morphologic parameters. Briefly, pre- and postcontrast scans were cropped to exclude nontumor regions in the analysis, intensity normalized, coregistered using nonrigid registration, and then subtracted (Fig. 1). Vessel structures were then segmented using a modified vesselness filter (27) and skeletonized using an iterative thinning algorithm (28) and an intensity-based gap filling model previously developed in our group (23). Because many cancer therapies are thought to normalize vascular structure in tumors, structural parameters such as vessel volume, branching points, diameter, length, and tortuosity were chosen to characterize morphologic changes (1). Total vessel volume was calculated by summing the voxels within segmentation, whereas the total number of branching points was calculated by summing the number of voxels in the skeleton with at least three adjacent skeleton voxels. Diameter was computed using a distance transform on the vessel segmentation, and tortuosity was computed as previously reported (29).

MR images were segmented and processed as previously described (30) to quantify functional parameters. Images from patients were corrected for motion using nonrigid image registration based on the Diffeomorphic Demons modified by use of the Normalized Gradient Fields and the adaptive regularization scheme (31). Details of the current implementation are described elsewhere. Because preclinical tumors were imaged with a surface coil to avoid motion, only voxels with K values > 0.6 were analyzed because of the limited depth of penetration of the surface coil. Beyond this distance, the signal-to-noise was unacceptable and the T1 mapping calculation began to break down (Supplementary Fig. S1A and S1B). The initial area under the curve ($i\text{AUC}_{90}$) was calculated by integrating the gadolinium (Gd) concentration curve up to the first 90 seconds after injection. K^{trans} was calculated from the Tofts model (32) using a population-averaged arterial input function (33) for preclinical tumors and was calculated using PKView software (34) for clinical tumors. We also quantified a third MR parameter, the fraction of voxels that enhanced at the first time point after injection (BAT_{frac}). Although this parameter is not frequently used, it is calculated independent of pharmacokinetic models and is sensitive to changes induced by cancer therapy (30). The tumor was split into two regions, rim (1/3 of the tumor volume) and core (2/3 of the volume) for spatial analysis of signal. These values were chosen because previous reports highlighted radial heterogeneity in these tumor regions (30).

Measurement of vessel density *ex vivo*

In vivo measurements of vessel density were confirmed using *ex vivo* sections of tumors.

Immunofluorescence staining was performed on tissue sections to quantify perfused vessel coverage per viable tissue area and pericyte coverage, and hematoxylin and eosin (H&E) staining was performed to confirm necrosis. Because perfused vessels were already labeled with CD31 (officially known as PECAM-1), only staining against the pericyte marker NG2 (officially known as chondroitin sulfate proteoglycan 4) was performed. Sections containing the entire tumor were imaged using fluorescence microscopy (Nikon Ti-E, Nikon Instruments Europe B.V.), and staining was quantified using an automated algorithm, as previously described (35). Further details regarding staining and quantification are provided in Supplementary Methods.

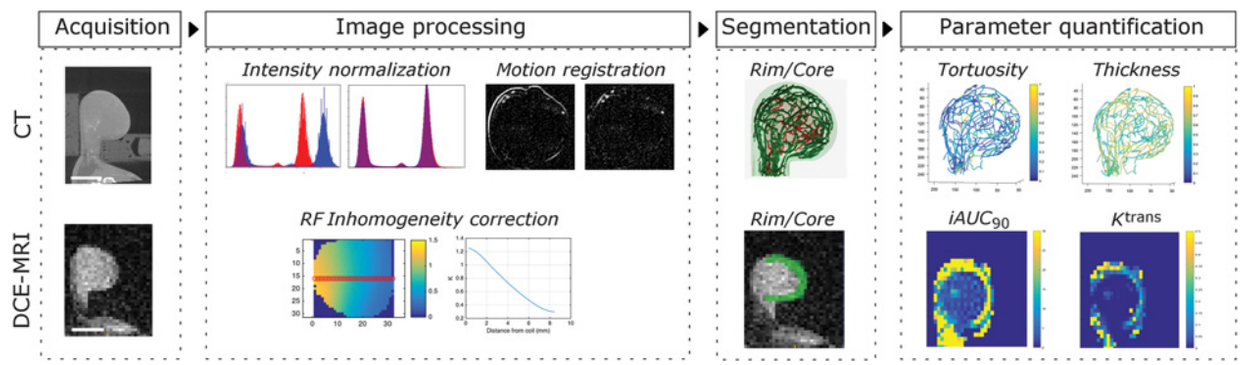

Figure 1.

Schematic illustrating acquisition and analysis pipeline from multimodal imaging of vessel structure and tumor perfusion. After immobilization in holder, tumors were imaged sequentially using CT and DCE-MRI. Pre- and postcontrast images from CT were intensity normalized and corrected for motion using nonrigid registration, whereas those from MRI were corrected for RF inhomogeneity and normalized to injected gadolinium concentration. Once vessels and tumor regions were extracted using segmentation algorithms, structural and functional parameters were quantified.

Statistical analysis

We fit linear models using ordinary least square regression (R Project, v. 3.4) to test the dependency of each MR parameter on CT parameters. For mouse tumors, linear models for $iAUC_{90}$, K^{trans}, and BAT_{frac} were generated using data from the cohort of mice from cohort 1. To simplify statistical analysis, the median value from log-transformed histograms of each imaging parameter was used for each mouse. We tested the dependence of each MR parameter on the following parameters: tumor region, tumor type, vessel volume, vessel radius, and vessel tortuosity. Because vessel volume, branching points, and vessel length were all strongly, linearly correlated (Pearson $R^2 = 0.97$) with one another, and because vessel volume correlated with tumor volume (Pearson $R^2 = 0.91$), we used only vessel volume in the model search to avoid violating the assumption that variables in linear models are independent.

An initial model search was performed to select the model that minimized the Bayesian information criterion. Model searches were performed using the stepAIC function in R (v. 3.4), where the search was initialized from a model containing all main effects. The scope of the search contained all main effects and all possible interaction effects. StepAIC was allowed to add and subtract effects. Residuals were checked for homoscedasticity, normality, and outliers. After linear models were chosen for cohort 1, they were then applied to cohort 2. To test reproducibility of the linear models, we applied the models on the imaging data from the control IgG–treated mice and evaluated them for goodness of fit using a sum of squares *F*-test, with a threshold of $P < 0.05$. To determine whether DC101 treatment had altered the relationships between vessel structure and function, the models were then applied to the imaging data from the DC101-treated mice and tested for goodness of fit. Finally, we performed a model search for $iAUC_{90}$ and K^{trans} to test whether the preclinical relationships held true for human tumors.

Results

In vivo quantification of vascular parameters indicates vascularity of preclinical tumor models

The methodology for *in vivo* validation of MR parameters was optimized in two preclinical tumor models known to produce different levels of vascularization (36, 37): mouse MC38 (high) and human FaDu (low). After tumors were imaged sequentially using CT and MRI, images were segmented into subregions (rim vs. core) to quantify spatial relationships between structural parameters (vessel volume, branch density, length, radius, and tortuosity) from CT images and functional parameters ($iAUC_{90}$, K^{trans}, and BAT_{frac}) from DCE-MR images (Fig. 1; Supplementary Fig. S1A and S1B). Repeated imaging of the same tumor during growth was not possible because the radiation dose from the CT scans was sufficient to curb tumor growth (Supplementary Fig. S2). Thus, we imaged untreated tumors (henceforth cohort 1) consisting of a range of volumes from each tumor model to investigate the dynamics of vessel structure and function.

Structural parameters derived from CT images reflected the degree of vascularity in the two tumor models. Although vessel volume was linearly correlated with tumor volume and with branch density in both tumor models (Fig. 2A and B), the degree of vascularization was significantly higher in MC38 than in FaDu (Fig. 2C). Other vascular parameters (vessel length, radius, and tortuosity) were also significantly higher in MC38 than in FaDu (Fig. 2D–F) and were poorly correlated with tumor volume (Supplementary Fig. S3). Nevertheless, we normalized for tumor volume in our subsequent analysis to avoid it being a confounding variable. Because the spatial resolution of the CT scan was 80 μm, we visualized perfused vessels (labeled with intravenously injected CD31) *ex vivo* to verify the degree of vascularization measured *in vivo* (where only perfused vessels were measured). MC38 tumor sections contained perfused vessels that were evenly distributed across entire tissue sections, whereas FaDu tumors contained perfused vessels in the periphery and contained large, central regions of necrosis (Fig. 2G). Vascular parameters (vessel/tumor volume, length, and radius) quantified from *ex vivo* sections corroborated the *in vivo* results (Fig. 2H–J), with the exception of vessel tortuosity, which was higher in *ex vivo* sections of FaDu tumors (Fig. 2K).

DCE-MR parameters of vessel function also reflected the degree of vascularity in the two tumor models. The parameter $iAUC_{90}$, which is used as a surrogate for tumor perfusion, was twofold higher in MC38 tumors than in FaDu tumors (Fig. 2L). Similar results were obtained for the parameter, K^{trans}, which is a composite measure of blood flow and vessel permeability (Fig. 2M). The parameter BAT_{frac}, reflecting the fraction of voxels that enhanced at the first time point after bolus injection, was fivefold higher in MC38 tumors than in FaDu tumors (Fig. 2N). Thus, these data confirm that the different levels of vascularization could be measured at both the structural and functional levels *in vivo*.

Functional MR parameters primarily reflect vessel density in preclinical tumors

Next, to determine whether functional MR parameters were linked to structural CT parameters in untreated tumors (cohort 1, Fig. 3A), vascular parameters extracted from the same tumor regions on CT and MR (Figs. 1 and 3B) were analyzed using linear models (Supplementary Fig. S4). The functional MR parameters, $iAUC_{90}$ (Fig. 3C) and K^{trans} (Fig. 3D), had a positive, linear relationship with vessel volume. However, vessel volume varied by both the tumor model ($P = 0.001$) and tumor subregion ($P = 3e{-}10$, Fig. 3C and D). No other structural parameter was found to significantly influence $iAUC_{90}$ or K^{trans} values in untreated tumors (Supplementary Table S1, equations 1–2). The MR parameter BAT_{frac} depended on vessel volume and radius (Supplementary Table S1, equation 3), and varied by tumor subregion and tumor model (Fig. 3E). Taken together, these results indicate that functional parameters are linked primarily to vessel density in untreated tumors and that this link varies by vascularity and subregion.

Antiangiogenic treatment alters functional–structural relationship in preclinical tumors

We then investigated whether antiangiogenic therapy alters the relationship between functional and structural parameters. Mice bearing the highly vascularized MC38 tumor (cohort 2) were imaged using CT and MR (Fig. 3F) after a course of IgG antibody or the anti-VEGFR2 receptor 2 antibody (DC101, 27 mg/kg). Treatment with DC101 significantly reduced tumor growth (Fig. 4A), reduced mean vessel length in the rim (Fig. 4B) and tortuosity in the core (Fig. 4C), and increased $iAUC_{90}$ values across the whole tumor ($F_{treatment}$ (1,42) = 4.88, $P = 0.026$; two-way ANOVA; Fig. 4D); it did not alter K^{trans} values (Fig. 4E). However, vessel volume (normalized to tumor volume) was not different

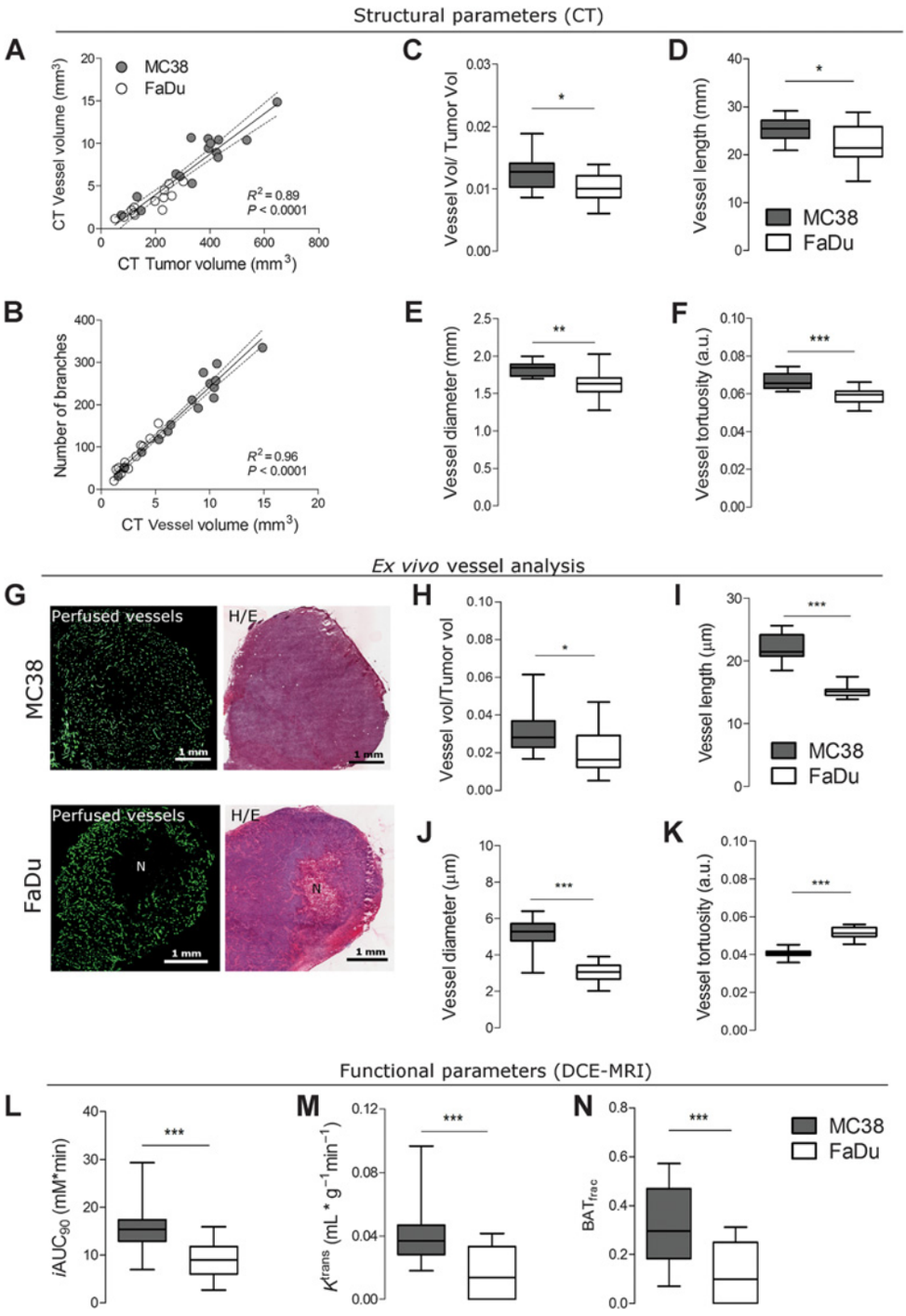

Figure 2.

Known differences in vessel structure and function can be measured using CT and DCE-MRI in two preclinical tumor models with different levels of vascularization. **A–F,** Structural vessel parameters (normalized vessel volume, branching points, length, diameter, and tortuosity) extracted from CT images from highly vascularized MC38 tumors and poorly vascularized FaDu tumors. Linear regressions are plotted with 95% confidence interval. **G,** Images of perfused vessels and H&E stains from MC38 tissue sections show even vessel distribution and negligible areas of necrosis (denoted by "N"), whereas those from FaDu tissue sections show uneven vessel distribution and regions of necrosis. **H–K,** Structural vessel parameters (normalized vessel volume, length, diameter, and tortuosity) quantified from whole *ex vivo* sections of MC38 and FaDu tumors. **L–N,** Functional parameters, $iAUC_{90}$ (mean initial area under the curve at 90 seconds after injection), K^{trans}, and BAT_{frac} (values of enhanced fraction at first time point after bolus injection) extracted from DCE-MRI images from MC38 and FaDu tumors. Box-whisker plots show median and percentiles (25th and 75th percentiles) as boxes, and minimum and maximum values as whiskers ($n = 16$ mice with MC38 tumors; $n = 13$ mice with FaDu tumors). *, $P < 0.05$; **, $P < 0.01$; and ***, $P < 0.001$ by unpaired t test with Welch correction.

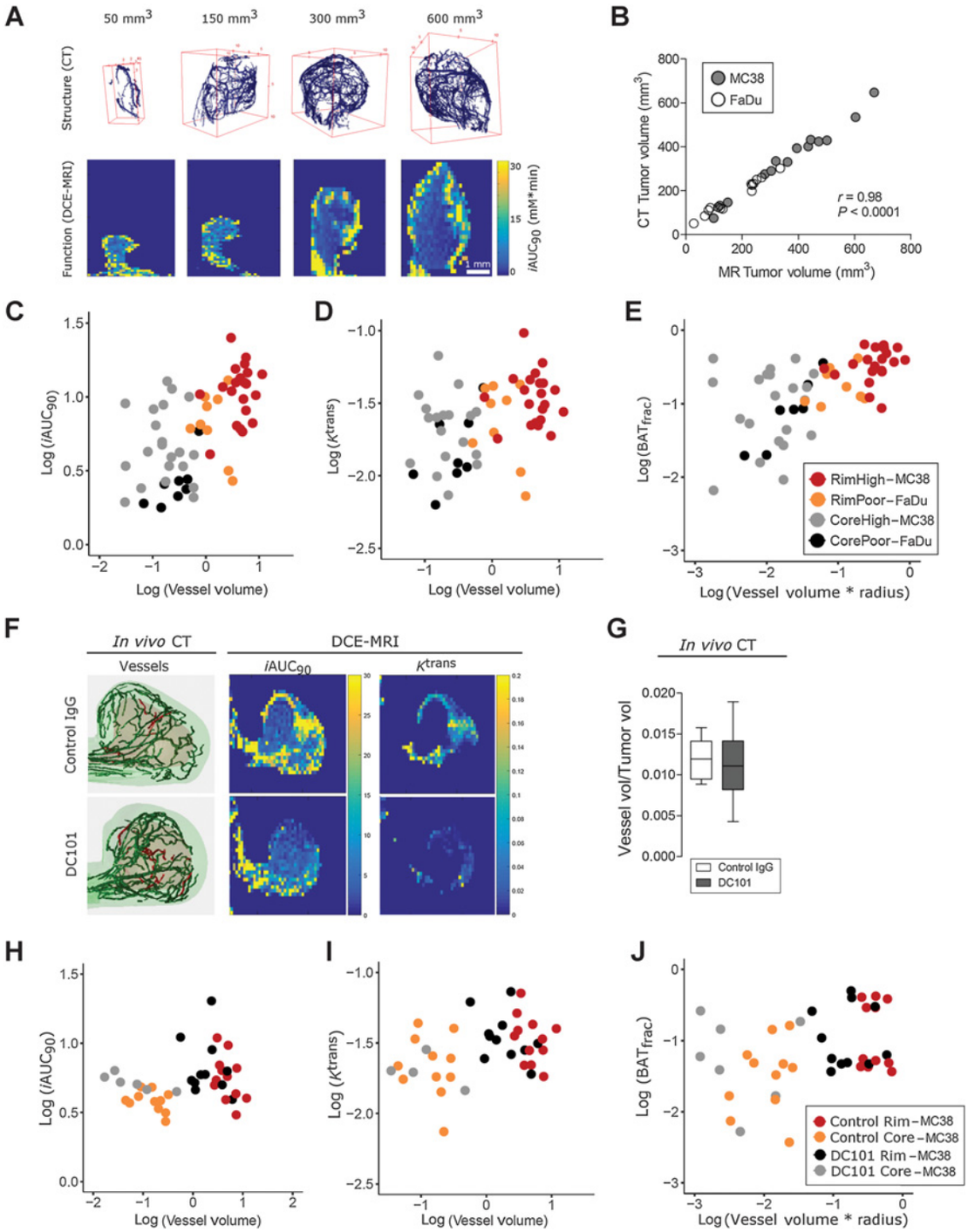

Figure 3.

Functional parameters of tumor perfusion reflect changes in vessel morphology in untreated preclinical tumors *in vivo* and have an altered relationship to vessel morphology after antiangiogenic treatment. **A,** Representative images of segmented vessels from CT and corresponding images of perfusion (*i*AUC) from a range of tumor volumes. **B,** Pearson correlation between analyzed tumor volume on CT and MRI images. **C–E,** Relationship of MR parameters, *i*AUC, K^{trans}, and BAT_{frac}, to morphologic parameters (vessel volume, tortuosity, and radius), tumor region (core vs. rim), and tumor type (MC38 "high" vs. FaDu "poor" vascularization), as identified by linear model analysis. **F,** Representative images of segmented vessels from CT and of MR images of *i*AUC (mmol/L * min) and K^{trans} (mL * g^{-1} * min^{-1}) from control and DC101-treated MC38 tumors. Green vessels are in the rim, whereas red vessels are in the core. Scale bar, 1 mm. **G,** Normalized vessel volume, as measured by CT, does not change with DC101 treatment. Box-whisker plots show median and percentiles (25th and 75th percentiles) as boxes, and minimum and maximum values as whiskers. **H–J,** Relationship of *i*AUC and BAT_{frac}, but not K^{trans}, with morphologic parameters is altered by DC101 treatment in MC38 tumors, as identified by linear model analysis.

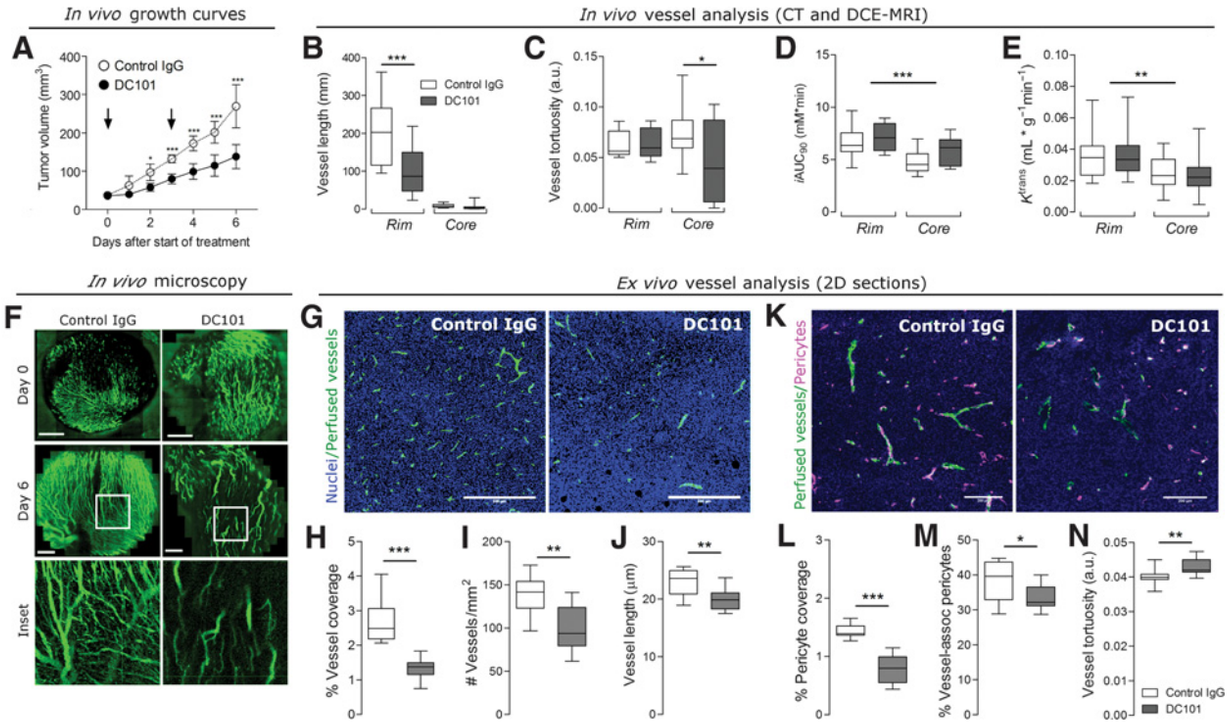

Figure 4.

Antiangiogenic treatment significantly affects tumor growth, and some morphologic and functional parameters in MC38 tumors. **A,** Treatment with the anti-VEGFR2 antibody, DC101 (27 mg/kg), slowed growth of MC38 tumors. Growth curves represent mean ± SD from one experiment ($n = 8$ mice/group). Control tumors were treated with IgG (27 mg/kg). Arrows indicate days on which mice were injected with antibodies. Scale bar, 5 cm. **B** and **C,** Treatment with the DC101 significantly decreased mean vessel length and tortuosity in the tumor rim and core, respectively. **D** and **E,** DC101 treatment significantly increased $iAUC_{90}$ across the whole tumor ($F_{treatment}$ (1,42) = 4.88, $P = 0.026$; two-way ANOVA) even though its effect could not be isolated to a specific subregion. In contrast, K^{trans} values were not significantly different between controls and treated groups. **F,** *In vivo* microscopy of perfused vessels visually confirms that DC101 destroys smaller vessels (10–50 μm, see inset) at the administered doses. **G,** Representative images of staining for nuclei (blue) and vessels (green) in control IgG– and DC101-treated tumors. Vessels shown are perfused; they were detected by i.v. injection of CD31-PE 10 minutes before tumor excision. Scale bar, 200 μm. **H–J,** Perfused vessel coverage (per viable tissue area), the number of perfused vessels per tumor area, and vessel length decrease with DC101 treatment. **K,** Representative images of staining for perfused vessels (green) and pericytes (magenta) in control IgG– and DC101-treated tumors. Vessels shown are perfused; they were detected by i.v. injection of CD31-PE 10 minutes before tumor excision. Scale bar, 200 μm. **L–N,** Pericyte coverage (per viable tissue area), the percentage of vessel-associated pericytes (detected by NG2), and vessel tortuosity measured *ex vivo* in control and DC101 tumor sections. Box-whisker plots show median and percentiles (25th and 75th percentiles) as boxes, and minimum and maximum values as whiskers. Data were pooled from two experiments ($n = 12$ mice total/group). *, $P < 0.05$; **, $P < 0.01$; and ***, $P < 0.01$ by one-way or two-way ANOVA followed by Bonferroni-corrected post *t* test or by Student *t* test with Welch correction (unpaired, two-tailed, $\alpha = 0.05$).

between the groups when measured by CT ($P = 0.48$, Fig. 3G). We used *in vivo* imaging of vessel perfusion using multiphoton microscopy to confirm that DC101 exerted an antiangiogenic effect (Fig. 4F). *Ex vivo* analysis of perfused vessels showed a 44% decrease in density, a 35% decrease in vessel number, and 16% decrease in vessel length in DC101-treated tumors (Fig. 4G–J), consistent with vascular regression. To assess whether features of vascular normalization were present, we measured pericyte coverage using NG2 in *ex vivo* sections (Fig. 4K). Treatment reduced pericyte coverage, the percentage of pericytes associated with vessels, and increased vessel tortuosity (Fig. 4L–N). These results confirm that DC101 exerted an antiangiogenic effect, although its effects were less prominent *in vivo* than *ex vivo*.

Antiangiogenic therapy changed the relationship between functional and structural parameters (Fig. 3H–J), as determined by the goodness of linear model fits (Supplementary Table S2; Supplementary Figs. S5 and S6). The dependency of $iAUC_{90}$ on vessel volume was reproducibly measured in control tumors ($P = 0.03$), but was not measured in DC101-treated tumors ($P = 0.204$; Supplementary Table S2, equation 1). A new model search for DC101-treated tumors was not significant at $\alpha = 0.05$, but it provides weak evidence of a relationship between $iAUC_{90}$ and vessel tortuosity ($P = 0.051$; Supplementary Table S2, equation 2). The model fit for the dependency of K^{trans} on vessel volume was not statistically significant in either control tumors ($P = 0.078$) or in DC101-treated tumors ($P = 0.145$; Supplementary Table S2, equation 3). The linear model for BAT_{frac} from cohort 1 showed a dependency of this parameter on both vessel volume and vessel radius. The dependencies partly reproduced in the control tumors of cohort 2 (vessel volume: $P = 0.009$; radius: $P = 0.241$), but not in the DC101-treated tumors of cohort 2 (vessel volume: $P = 0.34$; radius: $P = 0.60$; Supplementary Table S2, equation 4).

Functional parameters reflect vessel morphology in human tumors

Finally, to test whether this 3D biological validation strategy would be clinically feasible, we imaged 10 patients with

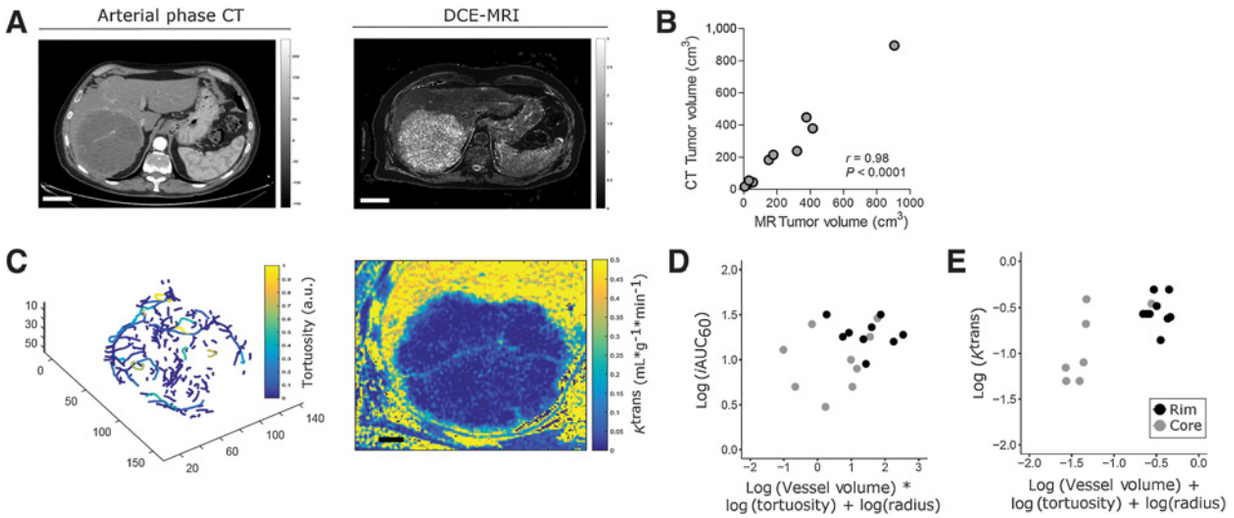

Figure 5.

Functional parameters depend on structural parameters in human tumors. **A,** Representative images from arterial phase CT and DCE-MRI scans from patients with liver metastases from colorectal cancer. Scale bar, 5 cm. **B,** Pearson correlation between tumor volumes segmented on MR and CT images. **C,** Representative images of vessel rendering and of K^{trans} maps from one metastatic lesion. **D** and **E,** Relationship of MR parameters, *i*AUC (mmol/L * min) and K^{trans} (mL * g^{-1} * min^{-1}), with morphologic parameters, as identified by linear model analysis.

chemorefractory liver metastases from colorectal cancer using arterial phase CT and DCE-MRI (Fig. 5A). Despite the images being acquired on different imaging scanners, tumor volumes segmented from both CT and MRI were significantly correlated (Fig. 5B). Analysis of vascular and functional parameters within lesions (Fig. 5C) revealed that MR parameters depended on structural parameters (Supplementary Table S3 and Supplementary Fig. S7), although the calculated relationships were more complex than those measured in preclinical tumors. We found that *i*AUC individually depended on vessel volume, radius, and tortuosity, as well as on the interaction among all the parameters (Fig. 5D; Supplementary Table S3, equation 1). That is, the parameters all modify each other's effect on *i*AUC. For example, for constant values of vessel radius and tortuosity, an increase in vessel volume would decrease *i*AUC. K^{trans} depended on vessel volume, radius, and tortuosity (Fig. 5E; Supplementary Table S3, equation 2). Thus, functional parameters reflect a combination of structural parameters in liver metastases.

Discussion

Use of vascular parameters from *in vivo* CT for validation of functional MR parameters

To improve imaging-biological validation of MR parameters, we developed a novel method that uses DCE-MRI and CT to measure the relationship between vessel function and structure *in vivo* and demonstrated feasibility of applying it to imaging of patients with cancer. Our method has detected key biological differences in vascular parameters of preclinical tumors across two tumor models and with antiangiogenic treatment and measured vascular parameters in patients with liver metastases from colorectal cancer. By linking functional MR parameters to specific aspects of vessel structure, our study provides information that can be used to inform the application of DCE-MRI in the clinic.

Using contrast-enhanced CT *in vivo*, we measured structural parameters such as vessel volume, radius, length, and tortuosity for vessels $\geq 80\,\mu m$ in preclinical tumors. Although this resolution does not allow for visualization of smaller vessels, we were nevertheless able to measure changes in vascular morphology. *In vivo* vascular parameters (vessel volume, length, and diameter) for the highly vascularized, untreated MC38 tumor model was significantly higher than in the poorly vascularized, untreated FaDu tumor model, consistent with *ex vivo* measurements of those parameters and with previous observations (36, 37). Vessel volume and branching density also increased linearly with tumor volume in accordance with previous data (38–40). Finally, when MC38 tumors were treated with DC101, significant changes in vessel tortuosity and vessel length were measured, consistent with previous reports on the effect of this antiangiogenic agent at this dose (24, 38). Together, our results show that most vascular parameters derived from *in vivo* CT are consistent with those obtained from *ex vivo* CT scans or microscopic imaging performed at higher resolutions (1–50 μm range, refs. 38, 40).

Although a few previous studies attempted to investigate the relationship between functional and structural parameters using multimodal imaging (41–43), the work performed here overcomes three methodological limitations of those studies. Firstly, we used 3D volumetric techniques in both our imaging modalities (DCE-MRI and CT), whereas previous studies used 2D regions of interest or 2D parameters for analysis of vessel structure, such as vessel surface area (41–43). As a result, volumetric analysis allowed us to analyze data from entire tumor regions as well as to perform spatial analysis based on tumor periphery and core—in line with recent consensus recommendations for biomarker validation (21). Secondly, our analysis was performed using improved alignment methods of multimodal images that substantially reduce motion artifacts in both preclinical and clinical tumors (22, 44). In contrast, previous studies did not correct for motion artifacts, which can cause misalignment in the images

from the different modalities and severely reduce the resolution of rendered vessels (22). Thirdly, the imaging was performed *in vivo*, avoiding the need to excise the tumor to image vessel architecture. It also demonstrates that structural and functional parameters, in principle, could be mapped *in vivo* in the same tumor over time to assess how and whether relationships change during the course of treatment. We have previously shown the value of including perfusion CT or DCE-MR in early-phase drug development of vasoactive agents (45). Although serial imaging using our approach would not be clinically possible due to the CT radiation dose, future work could use MRI sequences to improve imaging of vessel morphology without exposure to ionizing radiation (46).

Limitations of an *in vivo* approach to measuring structural–functional relationships

Given the restricted spatial resolution, one limitation of the *in vivo* method is that it likely only measures structural–functional relationships in larger vessels and, as such, has important implications in the use of *in vivo* imaging to determine these relationships. For example, the discordance in measurements of vessel volume and tortuosity obtained by CT versus microscopy in the DC101-treated tumors suggests that different vessel types (i.e., feeder vessels and arterioles in CT vs. capillaries in microscopy) were affected by treatment. Indeed, tumors have multiple types of vessels that stem from different growth mechanisms (47, 48), have different sizes, and respond differently to angiogenic factors such as VEGF (49). If changes induced by a treatment were to primarily affect the capillary level through sprouting or pruning, then the effect of treatment on structural–functional relationships would not be measured. However, for larger vessels (detectable within the scanner resolution) affected by treatment, the technique could offer insight into how antiangiogenics or other drugs alter vessel structure and tumor blood flow because the uptake of the contrast agents depends on blood supply to the tumor.

Relationships between functional and structural parameters of vessels

We found that the MR parameter *i*AUC primarily reflects the volume of perfused vessels in preclinical tumors. This was evidenced by results from cohorts 1 and 2, which both independently showed that *i*AUC had a positive, linear dependence on vessel volume that separated based on the tumor subregion. Antiangiogenic treatment likely affects this relationship because the model from untreated tumors of cohort 1 fit the control tumors of cohort 2, but not the DC101-treated tumors of cohort 2. Furthermore, a new model search suggested a positive, linear dependence between *i*AUC and vessel tortuosity in DC101-treated tumors of cohort 2. This change may have occurred due to a reduced number of smaller vessels (evidenced by the decrease in perfused vessels and in vessel-associated pericytes measured *ex vivo* in DC101-treated tumors), and/or due to vascular normalization of larger vessels (evidenced by an overall increase in $iAUC_{90}$ across the whole tumor in DC101-treated tumors and decrease in tortuosity measured in vivo). Published data suggest that vascular regression may be predominant at the time point of imaging (24, 25, 50), but our data also raise the possibility that treatment could affect smaller and larger vessels differently. A previous study suggested that *i*AUC and fractional blood volume may have a negative relationship in tumors treated with an antiangiogenic agent. However, as they were not able to measure the nature of the relationship in untreated tumors, we cannot assess whether antiangiogenic treatment affected the link between function and structure to make a meaningful comparison (43). Furthermore, control tumors in that study were imaged 3 days later than the treated tumors, when the tumor volume was twofold different between the two groups. We attempted to avoid these confounding factors by first establishing the relationship between $iAUC_{90}$ and structural parameters in a range of tumor volumes from untreated tumors, before testing these relationships in an independent cohort of tumors without and with treatment.

In liver metastases, *i*AUC reflected vascular parameters in a similar way (i.e., positive, linear dependence). However, we found a complex relationship in liver metastases between *i*AUC and CT parameters that has previously not been demonstrated. Prior studies from clinical work have shown conflicting relationships between *i*AUC and single vascular parameters such as microvessel density (4). Importantly, these analyses performed univariate comparisons, which cannot take into account interactions between variables. In contrast, the multivariate analysis presented here is sensitive to interactions between vascular parameters, and we find evidence of these interactions in human tumors. Although our preclinical data stem from tumors injected subcutaneously (for optimization of the imaging method and analysis algorithms), our preclinical and clinical findings suggest that *i*AUC may be linked to anatomical features of tumor vessels, which could provide some clarity on its biological interpretation.

Similar results were found for K^{trans}, which primarily reflected the vessel volume within our study. In preclinical tumors, K^{trans} had a positive, linear dependence on vessel volume in cohort 1 and was not reproduced with strong evidence in cohort 2, suggesting that the statistical power may not have been sufficient. As a result, we are unable to interpret the findings of the model fitting in the DC101-treated tumors in cohort 2, which also did not fit the initial model. We also did not measure any changes in K^{trans} with DC101 treatment in our study, possibly reflecting the variability in K^{trans} measurements or in biological response within individual tumors. Previous studies have shown that antiangiogenics decrease blood flow, decrease tortuosity, and normalize vessels (11, 15–17, 46, 51) that may have varied impact on functional MR parameters in a dose-dependent manner. At lower doses, antiangiogenic therapy can exert a vascular-normalizing effect that is expected to transiently increase perfusion and blood flow by reducing vessel density, leakiness, and/or tortuosity. However, at higher doses, treatment can exert a vascular-pruning effect that is expected to decrease blood flow and increase tortuosity, which are changes that would likely decrease *i*AUC and K^{trans} (2). These varied responses highlight the importance of assessing both the functional and structural effects of antiangiogenic therapy.

In patients with liver metastases, we also found that K^{trans} had a positive, linear dependence on a combination of three structural parameters including vessel volume, tortuosity, and radius. These results indicate that K^{trans}, which is often used as a functional surrogate for vessel permeability (21), may be affected by morphologic changes. Because the absolute value of K^{trans} varies between cases due to the parameter's reliance on pharmacokinetic model fitting, many studies report a change in K^{trans} when investigating therapeutic response. If K^{trans} reflected morphologic changes, then it would potentially eliminate the need to quantify change and instead could provide a value that can be linked to morphologic features.

The last MR parameter we investigated, BAT_{frac}, had mixed linear dependencies to vascular parameters in preclinical cohort 1. The parameter dependencies were partly reproduced in cohort 2, but all dependencies were lost with DC101 treatment, consistent with observations for the other two MR parameters. Although this parameter is not used clinically, we previously showed that it was sensitive to changes induced by radiotherapy (30). Furthermore, because it does not require pharmacokinetic modeling, it would be easier to use if these relationships are reproduced in clinical scenarios.

Potential translational impact of study

DCE-MRI parameters, *i*AUC and K^{trans}, have been used as imaging biomarkers to predict tumor response to antiangiogenic therapies, but how these parameters reflect changes at the vascular level has been unclear. We performed multimodal imaging to determine whether MR imaging biomarkers of vascular function could be linked to structural features of tumor vessels *in vivo*. Our preclinical and clinical data demonstrate that MR parameters have a relationship to structural features, that the relationship varies by tumor region and vascularity, and that it is affected by antiangiogenic therapy. By coupling functional parameters to structural ones, this *in vivo* method could potentially provide insight into why antiangiogenic therapies have varied functional responses and as such could potentially improve the use of these imaging biomarkers in clinical decision-making in assessing the effect of antiangiogenic therapies.

Disclosure of Potential Conflicts of Interest

P. Kannan and immediate family members of W.W. Kretzschmar are consultant/advisory board members for Avaant Imaging Inc. J.A. Schnabel reports receiving other commercial research support from Perspectum Diagnostics Ltd. No potential conflicts of interest were disclosed by the other authors.

Authors' Contributions

Conception and design: P. Kannan, J. Kaeppler, B. Markelc, S. Smart, T. Maughan, A.L. Harris, R.A. Sharma, V. Kersemans

Development of methodology: P. Kannan, W.W. Kretzschmar, D. Warren, B. Irving, B. Markelc, P. Kinchesh, S. Gilchrist, S. Smart, J.A. Schnabel, M. Partridge, V. Kersemans

Acquisition of data (provided animals, acquired and managed patients, provided facilities, etc.): P. Kannan, H. Winter, P.D. Allen, N. Syed, J. Kaeppler, B. Markelc, P. Kinchesh, S. Gilchrist, S. Smart, V. Kersemans

Analysis and interpretation of data (e.g., statistical analysis, biostatistics, computational analysis): P. Kannan, W.W. Kretzschmar, H. Winter, D. Warren, R. Bates, P.D. Allen, B. Irving, B.W. Papiez, B. Markelc, S. Smart, J.A. Schnabel, A.L. Harris, M. Partridge, R.A. Sharma, V. Kersemans

Writing, review, and/or revision of the manuscript: P. Kannan, W.W. Kretzschmar, H. Winter, D. Warren, J. Kaeppler, B. Markelc, S. Gilchrist, S. Smart, J.A. Schnabel, T. Maughan, A.L. Harris, R.J. Muschel, M. Partridge, R.A. Sharma, V. Kersemans

Administrative, technical, or material support (i.e., reporting or organizing data, constructing databases): P. Kannan, D. Warren, N. Syed, S. Gilchrist, M. Partridge, V. Kersemans

Study supervision: H. Winter, S. Smart, J.A. Schnabel, T. Maughan, R.J. Muschel, V. Kersemans

Acknowledgments

This research was supported by the Medical Research Council and Cancer Research UK (grant numbers C5255/A12678 and C2522/A10339). P. Kannan, H. Winter, N. Syed, R. Bates, P.D. Allen, B. Irving, B.W. Papiez, J. Kaeppler, B. Markelc, P. Kinchesh, S. Gilchrist, S. Smart, M. Partridge, R.J. Muschel, T. Maughan, A.L. Harris, R.A. Sharma, and V. Kersemans are funded by the CRUK/EPSRC Oxford Cancer Imaging Centre. W.W. Kretzschmar is funded by KTH Royal Institute of Technology. D. Warren is funded by CRUK (grant number: C5255/A15935). R.A. Sharma is funded by the NIHR University College London Hospitals Biomedical Research Centre and the UCL CRUK Experimental Cancer Medicines Centre.

We thank Dr. Graham Brown for assistance with microscopy (Microscopy Core Facility, Department of Oncology, University of Oxford), Dr. Phil Boardman (NHS, Churchill Hospital) for assistance with the clinical trial, and Biomedical Services Unit (University of Oxford).

The costs of publication of this article were defrayed in part by the payment of page charges. This article must therefore be hereby marked *advertisement* in accordance with 18 U.S.C. Section 1734 solely to indicate this fact.

Received January 15, 2018; revised May 11, 2018; accepted June 25, 2018; published first June 29, 2018.

References

1. Jain RK. Normalizing tumor microenvironment to treat cancer: bench to bedside to biomarkers. J Clin Oncol 2013;31:2205–18.
2. Carmeliet P, Jain RK. Principles and mechanisms of vessel normalization for cancer and other angiogenic diseases. Nat Rev Drug Discov 2011; 10:417–27.
3. Cuenod CA, Balvay D. Perfusion and vascular permeability: basic concepts and measurement in DCE-CT and DCE-MRI. Diagn Interv Imaging 2013;94:1187–204.
4. Jackson A, O'Connor JPB, Parker GJM, Jayson GC. Imaging tumor vascular heterogeneity and angiogenesis using dynamic contrast-enhanced magnetic resonance imaging. Clin Cancer Res 2007;13:3449–59.
5. Yang X, Knopp MV. Quantifying tumor vascular heterogeneity with dynamic contrast-enhanced magnetic resonance imaging: a review. J Biomed Biotechnol 2011;2011:1–12.
6. Kreisl TN, Zhang W, Odia Y, Shih JH, Butman JA, Hammoud D, et al. A phase II trial of single-agent bevacizumab in patients with recurrent anaplastic glioma. Neuro Oncol 2011;13:1143–50.
7. Sorensen AG, Batchelor TT, Zhang W-T, Chen P-J, Yeo P, Wang M, et al. A "vascular normalization index" as potential mechanistic biomarker to predict survival after a single dose of cediranib in recurrent glioblastoma patients. Cancer Res 2009;69:5296–300.
8. Liu G, Rugo HS, Wilding G, McShane TM, Evelhoch JL, Ng C, et al. Dynamic contrast-enhanced magnetic resonance imaging as a pharmacodynamic measure of response after acute dosing of AG-013736, an oral angiogenesis inhibitor, in patients with advanced solid tumors: results from a phase I study. J Clin Oncol 2005;23:5464–73.
9. Morgan B, Thomas AL, Drevs J, Hennig J, Buchert M, Jivan A, et al. Dynamic contrast-enhanced magnetic resonance imaging as a biomarker for the pharmacological response of PTK787/ZK 222584, an inhibitor of the vascular endothelial growth factor receptor tyrosine kinases, in patients with advanced colorectal cancer and liv. J Clin Oncol 2003;21: 3955–64.
10. Lee L, Sharma S, Morgan B, Allegrini P, Schnell C, Brueggen J, et al. Biomarkers for assessment of pharmacologic activity for a vascular endothelial growth factor (VEGF) receptor inhibitor, PTK787/ZK 222584 (PTK/ZK): translation of biological activity in a mouse melanoma metastasis model to phase I studies in patients with. Cancer Chemother Pharmacol 2006;57:761–71.
11. Wedam SB, Low JA, Yang SX, Chow CK, Choyke P, Danforth D, et al. Antiangiogenic and antitumor effects of bevacizumab in patients with inflammatory and locally advanced breast cancer. J Clin Oncol 2006; 24:769–77.
12. Baar J, Silverman P, Lyons J, Fu P, Abdul-Karim F, Ziats N, et al. A vasculature-targeting regimen of preoperative docetaxel with or without bevacizumab for locally advanced breast cancer: impact on angiogenic biomarkers. Clin Cancer Res 2009;15:3583–90.
13. Sweis R, Medved M, Towey S, Karczmar GS, Oto A, Szmulewitz RZ, et al. Dynamic contrast-enhanced magnetic resonance imaging as a pharmacodynamic biomarker for pazopanib in metastatic renal carcinoma. Clin Genitourin Cancer 2017;15:207–12.
14. Choi SH, Jung SC, Kim KW, Lee JY, Choi Y, Park SH, et al. Perfusion MRI as the predictive/prognostic and pharmacodynamic biomarkers in recurrent

malignant glioma treated with bevacizumab: a systematic review and a time-to-event meta-analysis. J Neurooncol 2016;128:185–94.
15. Flaherty KT, Hamilton BK, Rosen MA, Amaravadi RK, Schuchter LM, Gallagher M, et al. Phase I/II trial of imatinib and bevacizumab in patients with advanced melanoma and other advanced cancers. Oncologist 2015;20:952–9.
16. Guo J, Glass JO, McCarville MB, Shulkin BL, Daryani VM, Stewart CF, et al. Assessing vascular effects of adding bevacizumab to neoadjuvant chemotherapy in osteosarcoma using DCE-MRI. Br J Cancer 2015;113:1282–8.
17. Kim Y-E, Joo B, Park M-S, Shin SJ, Ahn JB, Kim M-J. Dynamic contrast-enhanced magnetic resonance imaging as a surrogate biomarker for bevacizumab in colorectal cancer liver metastasis: a single-arm, exploratory trial. Cancer Res Treat 2016;48:1210–21.
18. O'Connor JPB, Rose CJ, Waterton JC, Carano RAD, Parker GJM, Jackson A, et al. Imaging intratumor heterogeneity: role in therapy response, resistance, and clinical outcome. Clin Cancer Res 2014;21:249–57.
19. Yankeelov TE, Abramson RG, Quarles CC. Quantitative multimodality imaging in cancer research and therapy. Nat Rev Clin Oncol 2014;11:670–80.
20. Emblem KE, Mouridsen K, Bjornerud A, Farrar CT, Jennings D, Borra RJH, et al. Vessel architectural imaging identifies cancer patient responders to anti-angiogenic therapy. Nat Med 2013;19:1178–83.
21. O'Connor JPB, Aboagye EO, Adams JE, Aerts HJ, Barrington SF, Beer AJ, et al. Imaging biomarker roadmap for cancer studies. Nat Rev Clin Oncol 2017;14:169–86.
22. Kersemans V, Kannan P, Beech JS, Bates R, Irving B, Gilchrist S, et al. Improving in vivo high-resolution CT imaging of the tumour vasculature in xenograft mouse models through reduction of motion and bone-streak artefacts. PLoS One 2015;10:e0128537.
23. Bates R, Risser L, Irving B, Papiez BW, Kannan P, Kersemans V, et al. Filling large discontinuities in 3D vascular networks using skeleton- and intensity-based information. Med Image Comput Comput Interv 2015;9351:157–64.
24. Huang Y, Yuan J, Righi E, Kamoun WS, Ancukiewicz M, Nezivar J, et al. Vascular normalizing doses of antiangiogenic treatment reprogram the immunosuppressive tumor microenvironment and enhance immunotherapy. Proc Natl Acad Sci 2012;109:17561–6.
25. Prewett M, Huber J, Li Y, Santiago A, O'connor W, King K, et al. Antivascular endothelial growth factor receptor (Fetal Liver Kinase 1) monoclonal antibody inhibits tumor angiogenesis and growth of several mouse and human tumors. Cancer Res 1999;59:5209–18.
26. Wasan HS, Gibbs P, Sharma NK, Taieb J, Heinemann V, Ricke J, et al. First-line selective internal radiotherapy plus chemotherapy versus chemotherapy alone in patients with liver metastases from colorectal cancer (FOXFIRE, SIRFLOX, and FOXFIRE-Global): a combined analysis of three multicentre, randomised, phase 3 trials. Lancet Oncol 2017;18:1159–71.
27. Xiao C, Staring M, Shamonin D, Reiber JHC, Stolk J, Stoel BC. A strain energy filter for 3D vessel enhancement with application to pulmonary CT images. Med Image Anal 2011;15:112–24.
28. Lam L, Lee SW, Suen CY. Thinning methodologies - A comprehensive survey. IEEE Trans Pattern Anal Mach Intell 1992;869–85.
29. Bullitt E, Gerig G, Pizer SM, Lin W, Aylward SR. Measuring tortuosity of the intracerebral vasculature from MRA images. IEEE Trans Med Imaging 2003;22:1163–71.
30. Kleibeuker EA, Fokas E, Allen PD, Kersemans V, Griffioen AW, Beech J, et al. Low dose angiostatic treatment counteracts radiotherapy- induced tumor perfusion and enhances the anti-tumor effect. Oncotarget 2016;7:76613–27.
31. Papież BW, Heinrich MP, Fehrenbach J, Risser L, Schnabel JA. An implicit sliding-motion preserving regularisation via bilateral filtering for deformable image registration. Med Image Anal 2014;18:1299–311.
32. Tofts PS. Modeling tracer kinetics in dynamic Gd-DTPA MR imaging. J Magn Reson Imaging 1997;7:91–101.
33. Heilmann M, Walczak C, Vautier J, Dimicoli J-L, Thomas CD, Lupu M, et al. Simultaneous dynamic T1 and T2* measurement for AIF assessment combined with DCE MRI in a mouse tumor model. MAGMA 2007;20:193–203.
34. Irving B. maskSLIC: regional superpixel generation with application to local pathology characterisation in medical images. arXiv 2016;1606.09518.
35. Kannan P, Schain M, Kretzschmar WW, Weidner L, Mitsios N, Gulyás B, et al. An automated method measures variability in P-glycoprotein and ABCG2 densities across brain regions and brain matter. J Cereb Blood Flow Metab 2016;1–14.
36. Grimes DR, Kannan P, Markelc B, Bates R, Muschel RJ, Partridge M. Estimating oxygen distribution from vasculature in three-dimensional tumor tissue. J R Soc Interface 2016;13.
37. Kelly CJ, Hussien K, Fokas E, Kannan P, Shipley RJ, Ashton TM, et al. Regulation of O2 consumption by the PI3K and mTOR pathways contributes to tumor hypoxia. Radiother Oncol 2014;111:72–80.
38. Breckwoldt MO, Bode J, Kurz FT, Hoffmann A, Ochs K, Ott M, et al. Correlated magnetic resonance imaging and ultramicroscopy (MR-UM) is a tool kit to assess the dynamics of glioma angiogenesis. Elife 2016;5:1–17.
39. Dobosz M, Ntziachristos V, Scheuer W, Strobel S. Multispectral fluorescence ultramicroscopy: three- dimensional visualization and automatic quantification of tumor morphology, drug penetration, and antiangiogenic. Neoplasia 2014;16:1–13, W1–7.
40. Ehling J, Theek B, Gremse F, Baetke S, Möckel D, Maynard J, et al. Micro-CT imaging of tumor angiogenesis: quantitative measures describing micromorphology and vascularization. Am J Pathol 2014;184:431–41.
41. Reitan NK, Thuen M, Goa PE, de Lange Davies C. Characterization of tumor microvascular structure and permeability: comparison between magnetic resonance imaging and intravital confocal imaging. J Biomed Opt 2010;15:36004.
42. Gaustad J-V, Brurberg KG, Simonsen TG, Mollatt CS, Rofstad EK. Tumor vascularity assessed by magnetic resonance imaging and intravital microscopy imaging. Neoplasia 2008;10:354–62.
43. Kim E, Kim J, Maelandsmo GM, Johansen B, Moestue SA. Anti-angiogenic therapy affects the relationship between tumor vascular structure and function: A correlation study between micro-computed tomography angiography and dynamic contrast enhanced MRI. Magn Reson Med 2017;78:1513–22.
44. Papież BW, Franklin J, Heinrich MP, Gleeson FV, Schnabel JA. Liver motion estimation via locally adaptive over-segmentation regularization. In: Navab N, Hornegger J, Wells W, Frangi A, editors. Medical image computing and computer-assisted intervention. Springer; 2015. p.427–34.
45. Hill EJ, Roberts C, Franklin JM, Enescu M, West N, MacGregor TP, et al. Clinical trial of oral nelfinavir before and during radiation therapy for advanced rectal cancer. Clin Cancer Res 2016;22:1922–31.
46. Batchelor TT, Gerstner ER, Emblem KE, Duda DG, Kalpathy-Cramer J, Snuderl M, et al. Improved tumor oxygenation and survival in glioblastoma patients who show increased blood perfusion after cediranib and chemoradiation. Proc Natl Acad Sci U S A 2013;110:19059–64.
47. Pettersson A, Nagy JA, Brown LF, Sundberg C, Morgan E, Jungles S, et al. Heterogeneity of the angiogenic response induced in different normal adult tissues by vascular permeability factor/vascular endothelial growth factor. Lab Investig 2000;80:99–115.
48. Folberg R, Hendrix MJ, Maniotis AJ. Vasculogenic mimicry and tumor angiogenesis. Am J Pathol 2000;156:361–81.
49. Nagy JA, Chang S-H, Dvorak AM, Dvorak HF. Why are tumour blood vessels abnormal and why is it important to know? Br J Cancer 2009;100:865–9.
50. O'Connor JPB, Carano RAD, Clamp AR, Ross J, Ho CCK, Jackson A, et al. Quantifying antivascular effects of monoclonal antibodies to vascular endothelial growth factor: Insights from imaging. Clin Cancer Res 2009;15:6674–82.
51. Tolaney SM, Boucher Y, Duda DG, Martin JD, Seano G, Ancukiewicz M, et al. Role of vascular density and normalization in response to neoadjuvant bevacizumab and chemotherapy in breast cancer patients. Proc Natl Acad Sci U S A 2015;112:14325–30.